

Mutational signature in colorectal cancer caused by genotoxic *pks*⁺ *E. coli*

Cayetano Pleguezuelos-Manzano^{1,2,*}, Jens Puschhof^{1,2,*}, Axel Rosendahl Huber^{2,3,*}, Arne van Hoeck^{2,4}, Henry M. Wood⁵, Jason Nomburg^{6,7,8}, Carino Gurjao^{7,8}, Freek Manders^{2,3}, Guillaume Dalmaso⁹, Paul B. Stege¹⁰, Fernanda L. Paganelli¹⁰, Maarten H. Geurts^{1,2}, Joep Beumer¹, Tomohiro Mizutani^{1,2}, Reinier van der Linden¹, Stefan van Elst¹, Genomics England Research Consortium¹, Janetta Top¹⁰, Rob J.L. Willems¹⁰, Marios Giannakis^{7,8}, Richard Bonnet^{9,11}, Phil Quirke⁵, Matthew Meyerson^{7,8}, Edwin Cuppen^{2,4,12,13}, Ruben van Boxtel^{2,3,13}, Hans Clevers^{1,2,3,13}

1. Hubrecht Institute, Royal Netherlands Academy of Arts and Sciences (KNAW) and UMC Utrecht, 3584 CT Utrecht, The Netherlands.
2. Oncode Institute, Hubrecht Institute, 3584 CT Utrecht, The Netherlands.
3. The Princess Máxima Center for Pediatric Oncology, 3584 CS Utrecht, The Netherlands.
4. Center for Molecular Medicine and Oncode Institute, University Medical Centre Utrecht, Heidelberglaan 100, 3584CX, Utrecht, The Netherlands.
5. Pathology and Data Analytics, Leeds Institute of Medical Research at St James's, University of Leeds, Leeds, LS9 7TF, UK.
6. Graduate Program in Virology, Division of Medical Sciences, Harvard Medical School, 77 Avenue Louis Pasteur, Boston, MA 02115, USA.
7. Department of Medical Oncology, Dana-Farber Cancer Institute and Harvard Medical School, Boston, Massachusetts.
8. Broad Institute of MIT and Harvard, Cambridge, Massachusetts.
9. University Clermont Auvergne, Inserm U1071, INRA USC2018, M2iSH, F-63000, Clermont-Ferrand, France.
10. Department of Medical Microbiology, University Medical Center Utrecht, Utrecht, the Netherlands.
11. Department of Bacteriology, University Hospital of Clermont-Ferrand, Clermont-Ferrand, France.
12. Hartwig Medical Foundation, Amsterdam, The Netherlands.
13. CPCT consortium, Rotterdam, The Netherlands.

! Full author list at the end of the manuscript

* Co-first author
▣ Lead Contact

Correspondence: R.vanBoxtel@prinsesmaximacentrum.nl; h.clevers@hubrecht.eu

1 Abstract

2 Various species of the intestinal microbiota have been associated with the development
3 of colorectal cancer (CRC)^{1,2}, yet a direct role of bacteria in the occurrence of oncogenic
4 mutations has not been established. *Escherichia coli* can carry the pathogenicity island
5 *pks*, which encodes a set of enzymes that synthesize colibactin³. This compound is
6 believed to alkylate DNA on adenine residues^{4,5} and induces double strand breaks in
7 cultured cells³. Here, we expose human intestinal organoids to genotoxic *pks*⁺ *Escherichia*
8 *coli* by repeated luminal injection over a period of 5 months. Whole genome sequencing
9 of clonal organoids before and after this exposure reveals a distinct mutational signature,
10 absent from organoids injected with isogenic *pks*-mutant bacteria. The same mutational
11 signature is detected in a subset of 5876 human cancer genomes from two independent
12 cohorts, predominantly in CRC. Our study describes a distinct mutational signature in CRC
13 and implies that the underlying mutational process directly results from past exposure to
14 bacteria carrying the colibactin-producing *pks* pathogenicity island.

15 The intestinal microbiome has long been suggested to be involved in colorectal cancer (CRC)
16 tumorigenesis^{1,2}. Various bacterial species are reportedly enriched in stool and biopsies of CRC
17 patients⁶⁻⁹, including genotoxic strains of *Escherichia coli* (*E. coli*)^{3,6,10,11}. The genome of these
18 genotoxic *E. coli* harbors a 50 kb hybrid polyketide-nonribosomal peptide synthase operon (*pks*,
19 also referred to as *clb*) responsible for the production of the genotoxin colibactin. *pks*⁺ *E. coli* are
20 present in a significant fraction of individuals (~20% healthy individuals, ~40% inflammatory bowel
21 disease, ~60% familial adenomatous polyposis and CRC)^{6,10,11}. *pks*⁺ *E. coli* induce - amongst
22 others - interstrand crosslinks (ICLs) and double strand breaks (DSBs) in epithelial cell lines^{3,10-}
23 ¹² and in gnotobiotic mouse models of CRC, in which they can also contribute to
24 tumorigenesis^{6,10,11}. Recently, two studies have reported colibactin-adenine adducts, which are
25 formed in mammalian cells exposed to *pks*⁺ *E. coli*^{4,5}. While the chemistry of colibactin's
26 interaction with DNA is thus well-established, the outcome of this process in terms of recognizable
27 mutations remains to be determined. Recent advances in sequencing technologies and the
28 application of novel mathematical approaches allow classification of somatic mutational patterns.
29 Stratton and colleagues have pioneered a mutational signature analysis which includes the bases
30 immediately 5' and 3' to the single base substitution (SBS), and a number of different contexts
31 characterizing insertions and deletions (indels)^{13,14}. More than 50 mutational signatures have thus
32 been defined in cancers. For some, the underlying causes (e.g. tobacco smoke, UV light, specific
33 genetic DNA repair defects) are known^{13,15,16}. However, for many the underlying etiology remains
34 unclear. Human intestinal organoids, established from primary crypt stem cells¹⁷, have been
35 useful to identify underlying causes of mutational signatures¹⁸: After being exposed to a specific
36 mutational agent in culture, the organoids can be subcloned and analyzed by Whole Genome
37 Sequencing (WGS) to reveal the consequent mutational signature^{16,19,20}.

38 In order to define the mutagenic characteristics of *pks*⁺ *E. coli*, we developed a co-culture protocol
39 in which a *pks*⁺ *E. coli* strain (originally derived from a CRC biopsy²¹) was microinjected into the
40 lumen of clonal human intestinal organoids²² (Fig. 1a, b). An isogenic *clbQ* knock-out strain,
41 incapable of producing active colibactin^{21,23}, served as negative control. Both bacterial strains
42 were viable for at least 3 days in co-culture and followed similar growth dynamics (Fig. 1c). DSBs
43 and ICLs, visualized by γ H2AX and FANCD2 immunofluorescence, were induced specifically in
44 epithelial cells exposed to *pks*⁺ *E. coli* (Fig. 1d, e, Extended Data Fig. 1a), confirming that *pks*⁺ *E.*
45 *coli* induced DNA damage in our model. This co-culture induced no significant viability difference
46 between organoids exposed to *pks*⁺ and *pks* Δ *clbQ* *E. coli*, although there was a modest decrease
47 when compared to the dye-only injected organoids (Extended Data Fig. 1b, c). We then performed
48 repeated injections (with *pks*⁺ *E. coli*, *pks* Δ *clbQ* *E. coli* or dye-only) into single cell-

49 derived organoids, in order to achieve long-term exposure over a period of 5 months.
50 Subsequently, sub-clonal organoids were established from individual cells extracted from the
51 exposed organoids. For each condition, three subclones were subjected to WGS (Fig. 2a). We
52 also subjected the original clonal cultures to WGS to subtract the somatic mutations that were
53 already present before co-culture. Organoids exposed to *pks*⁺ *E. coli* presented increased SBS
54 levels compared to *pks*Δ*clbQ*, with a bias towards T>N substitutions (Fig. 2b). These T>N
55 substitutions occurred preferentially at ATA, ATT and TTT (of which the middle base is mutated).
56 From this, we defined a *pks*-specific single base substitution signature (SBS-*pks*; Fig. 2c). This
57 mutational signature was not observed in organoids exposed to *pks*Δ*clbQ* *E. coli* or dye (Fig. 2b,
58 c, Extended Data Fig. 2a-c), proving this to be a direct consequence of the *pks*⁺ *E. coli* exposure.
59 Furthermore, exposure to *pks*⁺ *E. coli* induced a characteristic small indel signature (ID-*pks*),
60 which was characterized by single T deletions at T homopolymers (Fig. 2d, e, Extended Data Fig.
61 2d-f). SBS-*pks* and ID-*pks* were replicated in an independent human intestinal organoid line
62 (Extended Data Fig. 3a-d; SBS cosine similarity = 0.77; ID cosine similarity = 0.93) and with a
63 *clbQ*-knockout *E. coli* strain recomplemented with the *clbQ* locus (*pks*Δ*clbQ*:*clbQ*) (Extended Data
64 Fig. 3e-h; SBS cosine similarity = 0.95; ID cosine similarity = 0.95).

65 Next, we asked if the SBS-*pks* and ID-*pks* mutations were characterized by other recurrent
66 patterns. First, the assessed DNA stretch was extended beyond the nucleotide triplet. This
67 uncovered the preferred presence of an adenine residue 3bp upstream to the mutated SBS-*pks*
68 T>N site (Fig. 3a). Similarly, mutations that contributed to the ID-*pks* signature in poly-T stretches
69 showed an enrichment of adenines immediately upstream of the affected poly-T stretch (Fig. 3b).
70 Intriguingly, the lengths of the adenine stretch and the T-homopolymer were inversely correlated,
71 consistently resulting in a combined length of 5 or more A/T nucleotides (Extended Data Fig. 4a).
72 While SBS-*pks* and ID-*pks* are the predominant mutational outcomes of colibactin exposure, we
73 also observed longer deletions at sites containing the ID-*pks* motif in organoids treated with *pks*⁺
74 *E. coli* (Fig. 3c). Additionally, the SBS-*pks* signature exhibited a striking transcriptional strand bias
75 (Fig. 3d, e). We speculate that these observations reflect preferential repair of alkylated
76 adenosines on the transcribed strand by transcription-coupled nucleotide excision repair. These
77 features clearly distinguish the *pks* signature from published signatures of alkylating agents or
78 other factors¹⁹.

79 We then assessed if the experimentally deduced SBS-*pks* and ID-*pks* signatures occur in human
80 tumors by interrogating WGS data from a Dutch collection of 3668 solid cancer metastases²⁴. The
81 mutations a cancer cell has acquired at its primary site will be preserved even in metastases, so
82 that these provide a view on the entire mutational history of a tumor. We first performed non-
83 negative matrix factorization (NMF) on genome-wide mutation data obtained from 496 CRC
84 metastases in this collection. Encouragingly, this unbiased approach identified an SBS signature
85 that highly resembled SBS-*pks* (cosine similarity = 0.95; Extended Data Fig. 5a, b). We then
86 determined the contribution of SBS-*pks* and ID-*pks* to the mutations of each sample in the cohort.
87 This analysis revealed a strong enrichment of the two *pks* signatures in CRC-derived metastases
88 when compared to all other cancer types (Fisher's exact test p-value < 0.0001, Extended Data
89 Table 1), as is displayed for SBS-*pks* in Figure 4a and for ID-*pks* in Figure 4b. We noted 7.5%
90 SBS-*pks*, 8.8% ID-*pks* and 6.25% SBS/ID-*pks* high samples when applying a cutoff contribution
91 value at 0.05 (Extended Data Table 1, Fig. 4c). As expected, the SBS-*pks* and ID-*pks* signatures
92 were positively correlated in this metastasis dataset ($R^2 = 0.46$ (all samples); $R^2 = 0.70$ (CRC-
93 only); Fig. 4c), in line with their co-occurrence in our *in vitro* data set. The longer deletions at ID-
94 *pks* sites were also found to co-occur with SBS-*pks* and ID-*pks* (Fig. 4e, f). Additionally, we
95 evaluated the levels of the SBS-*pks* or ID-*pks* mutational signatures in an independent cohort,
96 generated in the framework of the Genomics England 100,000 Genomes Project. This dataset is
97 comprised of WGS data from 2208 CRC tumors, predominantly of primary origin. SBS-*pks* and

98 ID-*pks* were enriched in 5.0% and 4.4% of patients respectively, while 44 samples were high in
99 both SBS-*pks* and ID-*pks* (Fig. 4d). The relative contribution of both *pks*-signatures correlated
100 with an R² of 0.35 (Fig. 4d).

101 Finally, we also investigated to what extent the *pks* signatures can cause oncogenic mutations.
102 To this end, we investigated the most common driver mutations found in 7 CRC patient cohorts²⁵
103 for hits matching the extended SBS-*pks* or ID-*pks* target motifs (Fig. 3a, b). This analysis revealed
104 that 112 out of 4,712 (2.4%) CRC driver mutations matched the colibactin target motif
105 (Supplementary Table 1). *APC*, the most commonly mutated gene in CRC, contained the highest
106 number of mutations matching SBS-*pks* or ID-*pks* target sites, with 52 out of 983 driver mutations
107 (5.3%) matching the motifs (Fig. 4g). We then explored the mutations of the 31 SBS/ID-*pks* high
108 CRC metastases from the HMF cohort for putative driver mutations matching the extended motif.
109 In total, this approach detected 209 changes in protein coding sequences (displayed in
110 Supplementary Table 2). Remarkably, an identical *APC* driver mutation matching the SBS-*pks*
111 motif was found in two independent donors (Fig. 4h).

112 While this study was in revision, an article²⁶ was published describing the derivation of mutational
113 signatures from healthy human colon crypts. Stratton c.s. note the co-occurrence of two
114 mutational signatures in subsets of crypts from some of the subjects. These signatures were
115 termed SBS-A and ID-A. The authors derived hierarchical lineages of the sequenced crypts,
116 which allowed them to conclude that the -unknown- mutagenic agent was active only during early
117 childhood. Intriguingly, SBS-A and ID-A closely match SBS-*pks* and ID-*pks*, respectively. Our
118 data imply that *pks*⁺ *E. coli* is the mutagenic agent that is causative to the SBS-A and ID-A
119 signatures observed in healthy crypts. We assessed if the SBS-*pks* mutational signature
120 contributed early to the mutational load of metastatic samples from the Dutch cohort by evaluating
121 their levels separately in clonal (pre-metastasis) or non-clonal (post-metastasis) mutations. The
122 accumulation of SBS-*pks* and ID-*pks* at the primary tumor site or even earlier was substantiated
123 by the abundant presence of SBS-*pks* in clonal mutations in the cohort (Extended Data Fig. 5c).
124 In addition to CRCs, one head and neck- and three urinary tract-derived tumors from this cohort
125 also displayed a clear SBS-*pks* and ID-*pks* signature (Fig. 4c). Both tissues have been described
126 as sites of *E. coli* infection²⁷⁻²⁹. This rare occurrence of the *pks* signatures in non-CRC tumors
127 was substantiated by a preprint report³⁰ of signatures closely resembling SBS-*pks* and ID-*pks* in
128 an oral squamous cell carcinoma patient.

129 The distinct motifs at sites of colibactin-induced mutations may serve as a starting point for deeper
130 investigations into the underlying processes. Evidence is accumulating that colibactin forms
131 interstrand crosslinks between two adenosines^{4,5,12}, and our data imply a distance of 3-4 bases
132 between these adenosines. These crosslinks formed by a bulky DNA adduct could be resolved in
133 different ways, including induction of DSBs, Nucleotide Excision Repair or translesion synthesis,
134 which in turn could result in various mutational outcomes. While our study unveils single base
135 substitutions and deletions as a mutational consequence, the underlying mechanisms will need
136 to be elucidated in more detailed DNA-repair studies.

137 In summary, we find that prolonged exposure of wild-type human organoids to genotoxic *E. coli*
138 allows the extraction of a unique SBS and indel signature. As organoids do not model
139 immune/inflammation effects or other microenvironmental factors, this provides evidence for
140 immediate causality between colibactin and mutations in the host epithelial cells. The adenine-
141 enriched target motif is in agreement with the proposed mode of action of colibactin's 'double-
142 warhead' attacking closely spaced adenine residues^{4,5,12}. The pronounced sequence specificity
143 reported here may inspire more detailed investigations on the interaction of colibactin with specific
144 DNA contexts. As stated above, Stratton and colleagues²⁶ likely describe SBS-*pks* and ID-*pks*

145 mutational signatures of the same etiology in primary human colon crypts. This agrees with the
146 notion that *pks*⁺ *E. coli*-induced mutagenesis indeed occurs in the healthy colon of individuals that
147 harbor genotoxic *E. coli* strains³¹ and that such individuals may be at an increased risk of
148 developing CRC. The small number of *pks* signature-positive urogenital and head-and-neck
149 cancer cases suggests that *pks*⁺ bacteria act beyond the colon. Intriguingly, presence of the *pks*
150 island in another strain of *E. coli*, Nissle 1917, is closely linked to its probiotic effect³². This strain
151 has been investigated for decades for diverse disease indications³³. Our data suggest that *E. coli*
152 Nissle 1917 may induce the characteristic SBS/ID-*pks* mutational patterns. Future research
153 should elucidate if this is the case *in vitro*, and in patients treated with *pks*⁺ bacterial strains. This
154 study implies that detection and removal of *pks*⁺ *E. coli*, as well as re-evaluation of probiotic strains
155 harboring the *pks* island, could decrease the risk of cancer in a large group of individuals.

156 METHODS

158 **Human material and organoid cultures**

160 Ethical approval was obtained from the ethics committees of the University Medical Center
161 Utrecht, Hartwig Medical Foundation and Genomics England. Written informed consent was
162 obtained from patients. All experiments and analyses were performed in compliance with relevant
163 ethical regulations.

164 **Organoid culture**

165 Clonal organoid lines were derived and cultured as described previously^{16,17}. In brief, wild type
166 human intestinal organoids (clonal lines ASC-5a and ASC-6a, previously used in Blokzijl *et al.*,³⁴)
167 were cultured in domes of Cultrex Pathclear Reduced Growth Factor Basement Membrane
168 Extract (BME) (3533-001, Amsbio) covered by medium containing Advanced DMEM/F12 (Gibco),
169 1x B27, 1x Glutamax, 10 mmol/L HEPES, 100 U/mL Penicillin-Streptomycin (all Thermo-Fisher),
170 1.25 mM N-acetylcysteine, 10 μM Nicotinamide, 10 μM p38 inhibitor SB202190 (all Sigma-
171 Aldrich) and the following growth factors: 0.5 nM Wnt Surrogate-Fc Fusion Protein, 2% Noggin
172 conditioned medium (both U-Protein Express), 20% Rspo1 conditioned medium (in-house), 50
173 ng/mL EGF (Peprotech), 0.5 μM A83-01, 1 μM PGE2 (both Tocris). For derivation of clonal lines,
174 cells were FACS sorted and grown at a density of 50 cells/μl in BME. 10 μM ROCK inhibitor Y-
175 27632 (Abmole, M1817) was added for the first week of growth. Upon reaching a size of >100 μm
176 diameter, organoids were picked and transferred to one well per organoid. All organoid lines were
177 regularly tested to rule out mycoplasma infection and authenticated using SNP profiling.

178 **Organoid bacteria co-culture**

179 The genotoxic *pks*⁺ *E. coli* strain was previously isolated from a CRC patient and isogenic
180 *pksΔclbQ* knock out and *pksΔclbQ:clbQ* recomplemented strains were generated based on this
181 strain²¹. Bacteria were initially cultured in Advanced DMEM (Gibco) supplemented with Glutamax
182 and HEPES to an O.D. of 0.4. They were then microinjected into the lumen of organoids as
183 previously described^{22,35}. Bacteria were injected at a multiplicity of infection of 1 together with
184 0.05% (w/v) FastGreen dye (Sigma) to allow tracking of injected organoids. At this point, 5 μg/mL
185 of the non-permeant antibiotic Gentamicin were added to the media to prevent overgrowth of
186 bacteria outside the organoid lumen. Cell viability was assessed as follows: Organoids were
187 harvested after 1, 3 or 5 days (bacteria were removed by primocin treatment at day 3) of co-
188 culture in cold DMEM (Gibco) and incubated in TrypLE Express (Gibco) at 37°C for 5 minutes
189 with repeated mechanical shearing. Single cells were resuspended in DMEM with added DAPI,
190 incubated on ice for at least 15 minutes and assessed for viability on a BD FACS Canto™. Cells
191 positive for DAPI were considered dead, while cells maintaining DAPI exclusion were counted as
192 viable. Bacterial growth kinetics were assessed by harvesting, organoid dissociation with 0.5%

193 saponin for 10 minutes and re-plating of serial dilutions on LB plates. Colony forming units were
194 quantified after overnight culture at 37°C. *E. coli* were killed with 1x Primocin (InvivoGen) after 3
195 days of co-culture, after which organoids were left to recover for 4 days before being passaged.
196 When the organoids reached a cystic stage again (typically after 2-3 weeks), the injection cycle
197 was repeated. This procedure was repeated 5 times (3 times for ASC Clone 6-a and the *clbQ*
198 recomplementation experiment in ASC Clone 5-a) to nivellate injection heterogeneity and ensure
199 accumulation of enough mutations for reliable signature detection.

200

201 **Whole-mount organoid immunofluorescence, DNA damage quantification and scanning** 202 **electron microscopy**

203 Organoids co-cultured with *pks⁺/pksΔclbQ E. coli*²¹ were collected in Cell Recovery Solution
204 (Corning) and incubated at 4°C for 30 minutes with regular shaking in order to free them from
205 BME. For FANCD2 staining, organoids were pre-permeabilized with 0.2% Triton-X (Sigma) for 10
206 minutes at room temperature. Then, organoids were fixed in 4% formalin overnight at 4°C.
207 Subsequently, organoids were permeabilized with 0.5% Triton-X (Sigma), 2% donkey serum
208 (BioRad) in PBS for 30 minutes at 4°C and blocked with 0.1% Tween-20 (Sigma) and 2% donkey
209 serum in PBS for 15 minutes at room temperature. Organoids were incubated with mouse anti-
210 γH2AX (Millipore; clone JBW301; 1:1000 dilution) or rabbit anti-FANCD2 (affinity purified in Pace
211 *et al.*³⁶; 1mg/ml) primary antibody overnight at 4°C. Then, organoids were washed 4 times with
212 PBS and incubated with either secondary goat anti-mouse AF-647 (Thermo Fisher, catalog
213 number A-21235, 1:500 dilution) or goat anti-rabbit AF-488 (Life Technologies, catalog number
214 A21206, 1:500 dilution) antibodies, respectively, for 3h at room temperature in the dark and
215 washed again with PBS. Organoids were imaged using an SP8 confocal microscope (Leica).
216 Fluorescent microscopic images of γH2AX foci were quantified as follows: Nuclei were classified
217 as containing either 0 or one or more foci. The fraction of nuclei containing foci over all nuclei is
218 displayed as one datapoint per organoid. Organoids co-cultured with bacteria for 24h were
219 harvested as described above and processed for scanning electron microscopy as previously
220 described³⁵.

221 **WGS and read alignment**

222 For WGS, clonal and subclonal cultures were generated for each condition. From these clonal
223 cultures DNA was isolated using the DNeasy Blood and Tissue Kit (Qiagen) using manufacturer's
224 instructions. Illumina DNA libraries were prepared using 50 ng of genomic DNA isolated from the
225 (sub-)clonal cultures isolated using TruSeq DNA Nano kit. The parental ASC 5a clone was
226 sequenced on a HiSeq XTEN instrument at 30x base coverage. All other samples were
227 sequenced using an Illumina Novaseq 6000 with 30x base coverage. Reads were mapped
228 against the human reference genome version GRCh37 by using Burrows-Wheeler Aligner³⁷
229 (BWA) version v0.7.5 with settings `bwa mem -c 100 -M`. Sequences were marked for duplicates
230 using Sambamba (v0.4.732) and realigned using GATK IndelRealigner (GATK version 3.4-46).
231 The full description and source code of the pipeline is available at
232 <https://github.com/UMCUGenetics/IAP>.

233 **Mutation calling and filtration**

234 Mutations were called using GATK Haplotypecaller (GATK version 3.4-46) and GATK
235 Queue producing a multi-sample Vcf file²⁰. The quality of the variants was evaluated using GATK
236 VariantFiltration v3.4-46 using the following settings: `-snpFilterName SNP_LowQualityDepth -`
237 `snpFilterExpression "QD < 2.0" -snpFilterName SNP_MappingQuality -snpFilterExpression "MQ`
238 `< 40.0" -snpFilterName SNP_StrandBias -snpFilterExpression "FS > 60.0" -snpFilterName`
239 `SNP_HaplotypeScoreHigh -snpFilterExpression "HaplotypeScore > 13.0" -snpFilterName`
240 `SNP_MQRankSumLow -snpFilterExpression "MQRankSum < -12.5" -snpFilterName`
241 `SNP_ReadPosRankSumLow -snpFilterExpression "ReadPosRankSum < -8.0" -snpFilterName`

```

242 SNP_HardToValidate -snpFilterExpression "MQ0 >= 4 && ((MQ0 / (1.0 * DP)) > 0.1)" -
243 snpFilterName SNP_LowCoverage -snpFilterExpression "DP < 5" -snpFilterName
244 SNP_VeryLowQual -snpFilterExpression "QUAL < 30" -snpFilterName SNP_LowQual -
245 snpFilterExpression "QUAL >= 30.0 && QUAL < 50.0 " -snpFilterName SNP_SOR -
246 snpFilterExpression "SOR > 4.0" -cluster 3 -window 10 -indelType INDEL -indelType MIXED -
247 indelFilterName INDEL_LowQualityDepth -indelFilterExpression "QD < 2.0" -indelFilterName
248 INDEL_StrandBias -indelFilterExpression "FS > 200.0" -indelFilterName
249 INDEL_ReadPosRankSumLow -indelFilterExpression "ReadPosRankSum < -20.0" -
250 indelFilterName INDEL_HardToValidate -indelFilterExpression "MQ0 >= 4 && ((MQ0 / (1.0 * DP))
251 > 0.1)" -indelFilterName INDEL_LowCoverage -indelFilterExpression "DP < 5" -indelFilterName
252 INDEL_VeryLowQual -indelFilterExpression "QUAL < 30.0" -indelFilterName INDEL_LowQual -
253 indelFilterExpression "QUAL >= 30.0 && QUAL < 50.0" -indelFilterName INDEL_SOR -
254 indelFilterExpression "SOR > 10.0.

```

255 **Somatic single base substitution and indel filtering**

256 To obtain high confidence catalogues of mutations induced during culture, we applied extensive
257 filtering steps previously described by Jager et al.²⁰. First, only variants obtained by GATK
258 VariantFiltration with a GATK phred-scaled quality score ≥ 100 for single base substitutions and
259 ≥ 250 for indels were selected. Subsequently, we only considered variants with at least 20x read
260 coverage in control and sample. We additionally filtered base substitutions with a GATK genotype
261 score (GQ) lower than 99 or 10 in WGS(t_n) or WGS(t_0), respectively. Indels were filtered when
262 GQ scores were higher than 60 WGS(t_n) or 10 in WGS(t_0). All variants were filtered against the
263 Single Nucleotide Polymorphism Database v137.b3730, from which SNPs present in the
264 COSMICv76 database were excluded. To exclude recurrent sequencing artefacts, we excluded
265 all variants variable in at least three individuals in a panel of bulk-sequenced mesenchymal
266 stromal cells³⁸. Next, all variants present at the start of co-culture (denominated WGS(t_0) in Fig.
267 2a) were filtered from those detected in the clonal *pks*⁺ *E. coli*, *pks* Δ *clbQ* *E. coli* co-cultures
268 (denominated WGS(t_n) in Fig. 2a) or dye culture. Indels were only selected when no called
269 variants in WGS(t_0) were present within 100bp of the indel and if not shared in WGS(t_0). In
270 addition, both indels and SNVs were filtered for the additional parameters: mapping quality (MQ)
271 of at least 60 and a variant allele (VAF) of 0.3 or higher to exclude variants obtained during the
272 clonal step. Finally, all multi-allelic variants were removed. Scripts used for filtering single base
273 substitutions (SNVFlv1.2) and indels (INDELFlv1.5) are deposited on
274 <https://github.com/ToolsVanBox/>.

275 **Mutational profile analysis**

276 In order to extract mutational signatures from the high-quality mutational catalogues after filtering,
277 we used the R package “MutationalPatterns” to obtain 96-trinucleotide single base substitution
278 and indel subcategory counts for each clonally cultured sample³⁹ (Extended Data Fig. 1a, d). In
279 order to obtain the additional mutational effects induced by *pks*⁺ *E. coli* (SBS and ID) we pooled
280 mutation numbers for each culture condition (*pks* Δ *clbQ* and *pks*⁺), and subtracted mutational
281 counts of *pks* Δ *clbQ* from *pks*⁺ (Fig. 2c, e, Extended Data Fig 2b, d). For the clones exposed to
282 *pks* Δ *clbQ*:*clbQ*, we subtracted relative levels of the *pks* Δ *clbQ* mutations in the same organoid
283 line. This enabled us to correct for the background of mutations induced by *pks* Δ *clbQ* *E. coli* and
284 injection dye. To determine transcriptional strand bias of mutations induced during *pks*⁺ *E. coli*
285 exposure, we selected all single base substitutions within gene bodies and checked whether the
286 mutated C or T was located on the transcribed or non-transcribed strand. We defined the
287 transcribed area of the genome as all protein coding genes based on Ensembl v75 (GCRh37)⁴⁰
288 and included introns and untranslated regions. The extended sequence context around mutation
289 sites was analyzed and displayed using an in-house script (“extended_sequence_context.R”). 2-
290 bit sequence motifs were generated using the R package “ggseqlogo”. Cosine similarities

291 between indel and single-base substitution profiles were calculated using the function
292 'cos_sim_matrix' from the MutationalPatterns package.

293

294 **Analysis of clonal mutations in the SBS/ID-*pks* high CRC tumors**

295 From the 31 SBS/ID-*pks* high CRC tumors clonal and subclonal single base substitutions were
296 defined to contain a purity/ploidy adjusted allele-fraction (PURPLE_AF) of < 0.4 or > 0.2,
297 respectively⁴¹. Signature re-fitting on both fractions was performed with the same signatures as
298 described above for the initial re-fitting of the HMF cohort.

299 **Analysis of >1bp deletions matching *pks*-motif**

300 For each > 1 bp T-deletion observed in organoid clones or the HMF cohort, the sequence of the
301 deleted bases and 5 base-pair flanking regions was retrieved using the R function "getSeq" from
302 the package "BSgenome". Retrieved sequences were examined for the presence of a 5 base-
303 pair motif matching the *pks*-motifs identified (Extended Data Fig. 4a) "AAAAT", "AAATT",
304 "AATTT" or "ATTTT". Sequences containing one or more matches with the motifs were marked
305 as positive for containing the motif.

306 **NMF extraction of signatures from HMF Colorectal cancer cohort**

307 In order to identify SBS-*pks* in an unbiased manner, signature extraction was performed on all
308 496 samples from colorectal primary tumors present in the HMF metastatic cancer database²⁴.
309 All variants containing the 'PASS' flag were used for analysis. Signature extraction was performed
310 using non-negative matrix factorization (NMF), using the R package "MutationalPatterns" function
311 "extract_signatures" with the following settings: rank = 17, nrun = 200. The cosine similarity of the
312 extracted signature matching SBS-*pks* was re-fitted to the COSMIC SigProfiler signatures and
313 SBS-*pks* was determined as described above to determine similarity (Extended Data Fig. 5a, b).

314 **Signature re-fitting on HMF cohort**

315 Mutation catalogues containing somatic variants processed according to Priestley et al, 2019
316 were obtained from the HMF. All variants containing the 'PASS' flag in the HMF dataset were
317 selected. Single base trinucleotide and indel subcategory counts were extracted using the R
318 package "MutationalPatterns" and in house-written R scripts respectively. In order to determine
319 the contribution of SBS-*pks* and ID-*pks* to these mutational catalogues, we re-fitted the COSMIC
320 SigProfiler mutational SBS and ID signatures v3 (<https://cancer.sanger.ac.uk/cosmic/signatures/>),
321 in combination with SBS-*pks* and ID-*pks*, to the mutational catalogues using the
322 MutationalPatterns function "fit_to_signatures". Signatures marked as possible sequencing
323 artefacts were excluded from the re-fitting. Cutoff values for high SBS-*pks* and ID-*pks* levels were
324 manually set at 5%, each. Numbers of SBS/ID-*pks* positive samples were compared between
325 CRC and other cancer types by Fisher's exact test (two-tailed).

326 **Mutation calling and filtration (Genomics England cohort)**

327 As part of the Genomics England 100,000 Genomes Project (main programme version 7)⁴²
328 standard pipeline, 2208 CRC genomes were sequenced on the Illumina HiSeq X platform. Reads
329 were aligned to the human genome (GRCh38) using the Illumina iSAAC aligner 03.16.02.1⁴³.
330 Mutations were called using Strelka and filtered in accordance with the HMF dataset²⁴.

331 Before examining somatic mutations for the *pks* mutational signature, mutation calls were first
332 subjected to additional filtering steps similar to those previously described²⁴. All calls present in
333 the matched normal sample were removed. The calls were split into high and low confidence
334 genomic regions according to lists available at [ftp://ftp-](ftp://ftp-trace.ncbi.nlm.nih.gov/giab/ftp/release/NA12878_HG001/NISTv3.3.1/GRCh38/)
335 [trace.ncbi.nlm.nih.gov/giab/ftp/release/NA12878_HG001/NISTv3.3.1/GRCh38/](ftp://ftp-trace.ncbi.nlm.nih.gov/giab/ftp/release/NA12878_HG001/NISTv3.3.1/GRCh38/). Somatic

336 mutation calls in high confidence regions were passed with a somatic score (QSI or QSS) of 10,
337 whilst calls in low confidence regions were passed with a score of 20. A pool of 200 normal
338 samples was constructed, and any calls present in three or more normal samples were removed.
339 Any groups of single nucleotide variants within 2bp were considered to be miss-called multiple
340 nucleotide variants and were removed. Finally, all calls had to pass the Strelka “PASS” filter.
341 Mutational signatures were then analysed as described above for the HMF cohort.
342

343 **Detection of *pks*-signature mutations in protein coding regions**

344 Mutations were extracted from the 31 SBS/ID-*pks* high CRC-samples. Exonic regions were
345 defined as all autosomal exonic regions reported in Ensembl v75 (GCRh37)⁴⁰. All extracted CRC
346 mutations were filtered for localization in exonic regions using the Bioconductor packages
347 “GenomicRanges”⁴⁴ and “BSgenome”. In a second filtering step, the sequence context of
348 mutations was required to match the following criteria:

349 For SBS-*pks*: T>N mutation, A or T directly upstream and downstream, A 3 bases upstream.

350 For ID-*pks*: Single T deletion, A directly upstream, a stretch of an A homopolymer followed by a
351 T polymer with combined length of at least 5 nucleotides, but no stretch exceeding 10 nucleotides
352 in length. Mutations passing both filter steps were further filtered for presence of a predicted
353 “HIGH” or “MODERATE” score in the transcript with highest impact score according to the
354 reported SnpEff annotation.

355 To assess the mutagenic impact of *pks*, we obtained all mutations from the 50 highest mutated
356 genes in CRC from IntOGen²⁵, release 2019.11.12. Mutations were filtered matching the *pks* motif
357 according to the sequence criteria stated above apart from the predicted impact score. Mutations
358 in *APC* were plotted using the R package “rtrackViewer”, using only exonic mutations.
359

360 REFERENCES

- 361 1. Allen, J. & Sears, C. L. Impact of the gut microbiome on the genome and epigenome of
362 colon epithelial cells: contributions to colorectal cancer development. *Genome Med.* **11**, 11
363 (2019).
- 364 2. Gagnaire, A., Nadel, B., Raoult, D., Neefjes, J. & Gorvel, J.-P. Collateral damage:
365 insights into bacterial mechanisms that predispose host cells to cancer. *Nat. Rev. Microbiol.*
366 **15**, 109–128 (2017).
- 367 3. Nougayrède, J.-P. *et al.* Escherichia coli Induces DNA Double-Strand Breaks in
368 Eukaryotic Cells. *Science* **313**, 848–851 (2006).
- 369 4. Wilson, M. R. *et al.* The human gut bacterial genotoxin colibactin alkylates DNA. *Science*
370 **363**, eaar7785 (2019).
- 371 5. Xue, M. *et al.* Structure elucidation of colibactin and its DNA cross-links. *Science* **365**,
372 eaax2685 (2019).
- 373 6. Dejea, C. M. *et al.* Patients with familial adenomatous polyposis harbor colonic biofilms
374 containing tumorigenic bacteria. *Science* **359**, 592–597 (2018).
- 375 7. Bullman, S. *et al.* Analysis of Fusobacterium persistence and antibiotic response in
376 colorectal cancer. *Science* **358**, 1443–1448 (2017).
- 377 8. Kostic, A. D. *et al.* Fusobacterium nucleatum potentiates intestinal tumorigenesis and
378 modulates the tumor-immune microenvironment. *Cell Host Microbe* **14**, 207–215 (2013).
- 379 9. Wirbel, J. *et al.* Meta-analysis of fecal metagenomes reveals global microbial signatures
380 that are specific for colorectal cancer. *Nat. Med.* **25**, 679 (2019).
- 381 10. Buc, E. *et al.* High prevalence of mucosa-associated E. coli producing cyclomodulin and
382 genotoxin in colon cancer. *PloS One* **8**, e56964 (2013).
- 383 11. Arthur, J. C. *et al.* Intestinal Inflammation Targets Cancer-Inducing Activity of the
384 Microbiota. *Science* **338**, 120–123 (2012).

- 385 12. Bossuet-Greif, N. *et al.* The Colibactin Genotoxin Generates DNA Interstrand Cross-
386 Links in Infected Cells. *mBio* **9**, (2018).
- 387 13. Alexandrov, L. B. *et al.* The Repertoire of Mutational Signatures in Human Cancer.
388 *Nature* **578**, 94–101 (2020).
- 389 14. Alexandrov, L. B. *et al.* Signatures of mutational processes in human cancer. *Nature*
390 **500**, 415–421 (2013).
- 391 15. Nik-Zainal, S. *et al.* Mutational processes molding the genomes of 21 breast cancers.
392 *Cell* **149**, 979–993 (2012).
- 393 16. Drost, J. *et al.* Use of CRISPR-modified human stem cell organoids to study the origin of
394 mutational signatures in cancer. *Science* **358**, 234–238 (2017).
- 395 17. Sato, T. *et al.* Long-term expansion of epithelial organoids from human colon, adenoma,
396 adenocarcinoma, and Barrett's epithelium. *Gastroenterology* **141**, 1762–1772 (2011).
- 397 18. Tuveson, D. & Clevers, H. Cancer modeling meets human organoid technology. *Science*
398 **364**, 952–955 (2019).
- 399 19. Kucab, J. E. *et al.* A Compendium of Mutational Signatures of Environmental Agents.
400 *Cell* **177**, 821-836.e16 (2019).
- 401 20. Jager, M. *et al.* Measuring mutation accumulation in single human adult stem cells by
402 whole-genome sequencing of organoid cultures. *Nat. Protoc.* **13**, 59–78 (2018).
- 403 21. Cougnoux, A. *et al.* Bacterial genotoxin colibactin promotes colon tumour growth by
404 inducing a senescence-associated secretory phenotype. *Gut* **63**, 1932–1942 (2014).
- 405 22. Bartfeld, S. *et al.* In Vitro Expansion of Human Gastric Epithelial Stem Cells and Their
406 Responses to Bacterial Infection. *Gastroenterology* **148**, 126-136.e6 (2015).
- 407 23. Li, Z.-R. *et al.* Divergent biosynthesis yields a cytotoxic aminomalonate-containing
408 precolibactin. *Nat. Chem. Biol.* **12**, 773–775 (2016).
- 409 24. Priestley, P. *et al.* Pan-cancer whole-genome analyses of metastatic solid tumours.
410 *Nature* **575**, 210–216 (2019).
- 411 25. Gonzalez-Perez, A. *et al.* IntOGen-mutations identifies cancer drivers across tumor
412 types. *Nat. Methods* **10**, 1081–1082 (2013).
- 413 26. Lee-Six, H. *et al.* The landscape of somatic mutation in normal colorectal epithelial cells.
414 *Nature* **574**, 532–537 (2019).
- 415 27. McLellan, L. K. & Hunstad, D. A. Urinary Tract Infection: Pathogenesis and Outlook.
416 *Trends Mol. Med.* **22**, 946–957 (2016).
- 417 28. Zawadzki, P. J. *et al.* Identification of infectious microbiota from oral cavity environment
418 of various population group patients as a preventive approach to human health risk factors.
419 *Ann. Agric. Environ. Med.* **23**, 566–569 (2016).
- 420 29. Banerjee, S. *et al.* Microbial Signatures Associated with Oropharyngeal and Oral
421 Squamous Cell Carcinomas. *Sci. Rep.* **7**, 4036 (2017).
- 422 30. Boot, A. *et al.* Mutational signature analysis of Asian OSCCs reveals novel mutational
423 signature with exceptional sequence context specificity. *bioRxiv* 368753 (2018)
424 doi:10.1101/368753.
- 425 31. Payros, D. *et al.* Maternally acquired genotoxic *Escherichia coli* alters offspring's
426 intestinal homeostasis. *Gut Microbes* **5**, 313–512 (2014).
- 427 32. Olier, M. *et al.* Genotoxicity of *Escherichia coli* Nissle 1917 strain cannot be dissociated
428 from its probiotic activity. *Gut Microbes* **3**, 501–509 (2012).
- 429 33. Beimfohr, C. A Review of Research Conducted with Probiotic *E. coli* Marketed as
430 Symbioflor. *Int J Bacteriol* **2016**, 3535621 (2016).

431
432 REFERENCES FROM METHODS SECTION

- 433 34. Blokzijl, F. *et al.* Tissue-specific mutation accumulation in human adult stem cells during
434 life. *Nature* **538**, 260–264 (2016).
- 435 35. Heo, I. *et al.* Modelling *Cryptosporidium* infection in human small intestinal and lung

- 436 organoids. *Nat. Microbiol.* **3**, 814–823 (2018).
- 437 36. Pace, P. *et al.* FANCE: the link between Fanconi anaemia complex assembly and
438 activity. *EMBO J.* **21**, 3414–3423 (2002).
- 439 37. Li, H. & Durbin, R. Fast and accurate long-read alignment with Burrows-Wheeler
440 transform. *Bioinforma. Oxf. Engl.* **26**, 589–595 (2010).
- 441 38. Osorio, F. G. *et al.* Somatic Mutations Reveal Lineage Relationships and Age-Related
442 Mutagenesis in Human Hematopoiesis. *Cell Rep.* **25**, 2308-2316.e4 (2018).
- 443 39. Blokzijl, F., Janssen, R., Boxtel, R. van & Cuppen, E. Mutational Patterns:
444 comprehensive genome-wide analysis of mutational processes. *Genome Med.* **10**, 1–11
445 (2018).
- 446 40. Cunningham, F. *et al.* Ensembl 2015. *Nucleic Acids Res.* **43**, D662-669 (2015).
- 447 41. Cameron, D. L. *et al.* GRIDSS, PURPLE, LINX: Unscrambling the tumor genome via
448 integrated analysis of structural variation and copy number. *bioRxiv* 781013 (2019)
449 doi:10.1101/781013.
- 450 42. The National Genomics Research and Healthcare Knowledgebase | Genomics England.
451 [https://www.genomicsengland.co.uk/the-national-genomics-research-and-healthcare-](https://www.genomicsengland.co.uk/the-national-genomics-research-and-healthcare-knowledgebase/)
452 [knowledgebase/](https://www.genomicsengland.co.uk/the-national-genomics-research-and-healthcare-knowledgebase/) (2017).
- 453 43. Racz, C. *et al.* Isaac: ultra-fast whole-genome secondary analysis on Illumina
454 sequencing platforms. *Bioinforma. Oxf. Engl.* **29**, 2041–2043 (2013).
- 455 44. Lawrence, M. *et al.* Software for Computing and Annotating Genomic Ranges. *PLoS*
456 *Comput. Biol.* **9**, (2013).

457 ACKNOWLEDGEMENTS

458 We thank Hoeijmakers J., Knipscheer P and Garaycochea J. for discussions on DNA damage.
459 We also thank Robinson P., and Vervier K., Lawley T., and Stratton M. for explorative analysis
460 and discussions.

461 This publication and the underlying study have been made possible partly on the basis of the data
462 that Hartwig Medical Foundation and the Center of Personalised Cancer Treatment (CPCT) have
463 made available to the study.

464 This research was made possible through access to the data and findings generated by the
465 100,000 Genomes Project. The 100,000 Genomes Project is managed by Genomics England
466 Limited (a wholly owned company of the Department of Health and Social Care). The 100,000
467 Genomes Project is funded by the National Institute for Health Research and NHS England. The
468 Wellcome Trust, Cancer Research UK and the Medical Research Council have also funded
469 research infrastructure. The 100,000 Genomes Project uses data provided by patients and
470 collected by the National Health Service as part of their care and support.

471 This work was supported by CRUK grant OPTIMISTIC [C10674/A27140], the Gravitation
472 projects CancerGenomiCs.nl and the Netherlands Organ-on-Chip Initiative (024.003.001) from
473 the Netherlands Organisation for Scientific Research (NWO) funded by the Ministry of Education,
474 Culture and Science of the government of the Netherlands (C.P.M, J.P.), the Onco Institute
475 (partly financed by the Dutch Cancer Society) the European Research Council under ERC
476 Advanced Grant Agreement no. 67013 (J.P., T.M, H.C.), a VIDI grant of the Netherlands
477 Organisation for Scientific Research (NWO) (no. 016.Vidi.171.023) to R.v.B (A.R.H.) and NWO
478 building blocks of life project: Cell dynamics within lung and intestinal organoids
479 (737.016.009)(M.H.G).

480

481 This work was supported by the Netherlands Organ-on-Chip Initiative, an NWO Gravitation
482 project (024.003.001) funded by the Ministry of Education, Culture and Science of the
483 government of the Netherlands
484

485 AUTHOR CONTRIBUTION

486 C.P.M., J.P., A.R.H. and H.C. conceived the study; C.P.M., J.P., A.R.H., R.vB. and H.C. wrote
487 the manuscript; A.R.H, H.W, F.M. and R.vB. performed signature analysis; A.R.H., A.vH., H.W.,
488 J.N., C.G., P.Q., M.G., M.M. and E.C. provided access to and analyzed patient WGS data; G.D.
489 and R.B. isolated bacterial strains and generated knockouts; C.P.M., J.P., T.M., R.vdL., M.H.G.
490 and S.vE. established and performed organoid cloning experiments; C.P.M., J.P. and J.B.
491 performed organoid co-culture experiments; P.S., F.P., J.T. and R.W. performed bacteria
492 validation and assays.

493 DATA AVAILABILITY STATEMENT

494
495 Whole-genome sequence data has been deposited in the European Genome-phenome Archive
496 (EGA; <https://ega-archive.org>); accession number EGAS00001003934. The data used from the
497 Hartwig Medical Foundation and Genomics England databases consist of patient-level somatic
498 variant data (annotated variant call data) and are considered privacy sensitive and available
499 through access-controlled mechanisms.

500
501 Patient-level somatic variant and clinical data have been obtained from the Hartwig Medical
502 Foundation under the data request number DR-084. Somatic variant and clinical data are freely
503 available for academic use from the Hartwig Medical Foundation through standardized
504 procedures. Privacy and publication policies, including co-authorship policies, can be retrieved
505 from: <https://www.hartwigmedicalfoundation.nl/en/data-policy/>. Data request forms can be
506 downloaded from <https://www.hartwigmedicalfoundation.nl/en/applying-for-data/>.
507 To gain access to the data, this data request form should be emailed
508 to info@hartwigmedicalfoundation.nl, upon which it will be evaluated within 6 weeks by the
509 HMF Scientific Council and an independent Data Access Board. When access is granted, the
510 requested data become available through a download link provided by HMF.

511
512 Somatic variant data from the Genomics England dataset was analyzed within the Genomics
513 England Research Environment secure data portal, under Research Registry project code RR87
514 and exported from the Research Environment following data transfer request 1000000003652 on
515 3rd December 2019.

516 The Genomics England dataset can be accessed by joining the community of academic and
517 clinical scientist via the Genomics England Clinical Interpretation Partnership
518 (GeCIP). <https://www.genomicsengland.co.uk/about-gecip/>. To join a GeCIP domain, the
519 following steps have to be taken:

- 520 1. Your institution has to sign the [GeCIP Participation Agreement](#), which outlines the key
521 principles that members of each institution must adhere to, including our Intellectual
522 Property and Publication Policy.
- 523 2. Submit your application using the relevant form found at the bottom of the page
524 (<https://www.genomicsengland.co.uk/join-a-gecip-domain/>).
- 525 3. The domain lead will review your application, and your institution will verify your identity
526 for Genomics England and communicate confirmation directly to Genomics England.

- 527 4. Your user account will be created.
- 528 5. You will be sent an email containing a link to complete Information Governance training
- 529 and sign the [GeCIP Rules \(https://www.genomicsengland.co.uk/wp-](https://www.genomicsengland.co.uk/wp-content/uploads/2019/07/GeCIP-Rules_29-08-2018.pdf)
- 530 [content/uploads/2019/07/GeCIP-Rules_29-08-2018.pdf](https://www.genomicsengland.co.uk/wp-content/uploads/2019/07/GeCIP-Rules_29-08-2018.pdf)). Completing the training and
- 531 signing the GeCIP Rules are requirements for you to access the data. After you have
- 532 completed the training and signed the rules, you will need to wait for your access to the
- 533 Research Environment to be granted.
- 534 6. This will generally take up to one working day. You will then receive an email letting you
- 535 know your account has been given access to the environment, and instructions for
- 536 logging in.

537 (for more detail, see: <https://www.genomicsengland.co.uk/join-a-gecip-domain/>)

538

539 Details of the data access agreement can be retrieved from:

540 https://figshare.com/articles/GenomicEnglandProtocol_pdf/4530893/5. All requests will be

541 evaluated by the Genomics England Access Review Committee taking into consideration patient

542 data protection, compliance with legal and regulatory requirements, resource availability and

543 facilitation of high quality research.

544 All analysis of the data must take place within the Genomics England Research Environment

545 secure data portal, <https://www.genomicsengland.co.uk/understanding-genomics/data/> and

546 exported following approval of a data transfer request.

547 Regarding co-authorship, all publications using data generated as part of the Genomics England

548 100,000 Genomes Project must include the Genomics England Research Consortium as co-

549 authors. The full publication policy is available at [https://www.genomicsengland.co.uk/about-](https://www.genomicsengland.co.uk/about-gecip/publications/)

550 [gecip/publications/](https://www.genomicsengland.co.uk/about-gecip/publications/).

551

552 All other data supporting the findings of this study are available from the corresponding author

553 upon request.

554 CODE AVAILABILITY

555 All analysis scripts are available on <https://github.com/ToolsVanBox/GenotoxicEcoli>.

556 CONFLICT OF INTEREST

557 The authors declare no conflict of interest.

558

559 GENOMICS ENGLAND RESEARCH CONSORTIUM AUTHOR LIST

560 Ambrose J. C. ¹, Arumugam P.¹, Baple E. L. ¹, Bleda M. ¹, Boardman-Pretty F. ^{1,2}, Boissiere J.

561 M. ¹, Boustred C. R. ¹, Brittain H.¹, Caulfield M. J.^{1,2}, Chan G. C. ¹, Craig C. E. H. ¹, Daugherty

562 L. C. ¹, de Burca A. ¹, Devereau, A. ¹, Elgar G. ^{1,2}, Foulger R. E. ¹, Fowler T. ¹, Furió-Tarí P. ¹,

563 Hackett J. M. ¹, Halai D. ¹, Hamblin A.¹, Henderson S.^{1,2}, Holman J. E. ¹, Hubbard T. J. P. ¹,

564 Ibáñez K.^{1,2}, Jackson R. ¹, Jones L. J. ^{1,2}, Kasperaviciute D. ^{1,2}, Kayikci M. ¹, Lahnstein L. ¹,

565 Lawson K. ¹, Leigh S. E. A. ¹, Leong I. U. S. ¹, Lopez F. J. ¹, Maleady-Crowe F. ¹, Mason J. ¹,

566 McDonagh E. M. ^{1,2}, Moutsianas L. ^{1,2}, Mueller M. ^{1,2}, Murugaesu N. ¹, Need A. C. ^{1,2}, Odhams

567 C. A. ¹, Patch C. ^{1,2}, Perez-Gil D. ¹, Polychronopoulos D. ¹, Pullinger J. ¹, Rahim T. ¹, Rendon

568 A. ¹, Riesgo-Ferreiro P.¹, Rogers T. ¹, Ryten M. ¹, Savage K. ¹, Sawant K. ¹, Scott R. H. ¹,

569 Siddiq A. ¹, Sieghart A. ¹, Smedley D. ^{1,2}, Smith K. R. ^{1,2}, Sosinsky A. ^{1,2}, Spooner W. ¹, Stevens

570 H. E. ¹, Stuckey A. ¹, Sultana R. ¹, Thomas E. R. A. ^{1,2}, Thompson S. R. ¹, Tregidgo C. ¹, Tucci
571 A. ^{1,2}, Walsh E. ¹, Watters, S. A. ¹, Welland M. J. ¹, Williams E. ¹, Witkowska K. ^{1,2}, Wood S. M.
572 ^{1,2}, Zarowiecki M. ¹.

573

574 1. Genomics England, London, UK

575 2. William Harvey Research Institute, Queen Mary University of London, London, EC1M 6BQ,
576 UK.

577

578 **Extended Data Table 1: SBS-*pks* and ID-*pks* levels across tissue types.** Sample
579 numbers are displayed by primary tumor type per row. Numbers of samples with more
580 than 5% contribution of either ID-*pks*, SBS-*pks* or both are shown; the proportion of
581 positive samples per tissue is indicated in brackets.
582

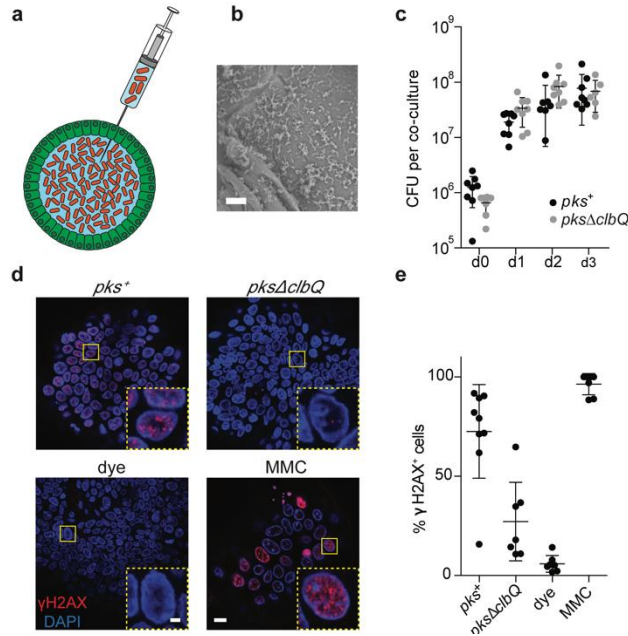
583 **Extended Data Table 1**

Primary Tumor Location	Total number	SBS- <i>pks</i> > 0.05	ID- <i>pks</i> > 0.05	SBS- <i>pks</i> > 0.05 & ID- <i>pks</i> > 0.05
CRC	496	37 (7,5%)	44 (8,8%)	31 (6,25%)
Head & Neck	61	1 (1,6%)	1 (1,6%)	1 (1,6%)
Urinary Tract	142	3 (2,1%)	6 (4,2%)	3 (2,1%)
Other	2969	12 (0,4%)	134 (4,5%)	1 (0,03%)

584

585

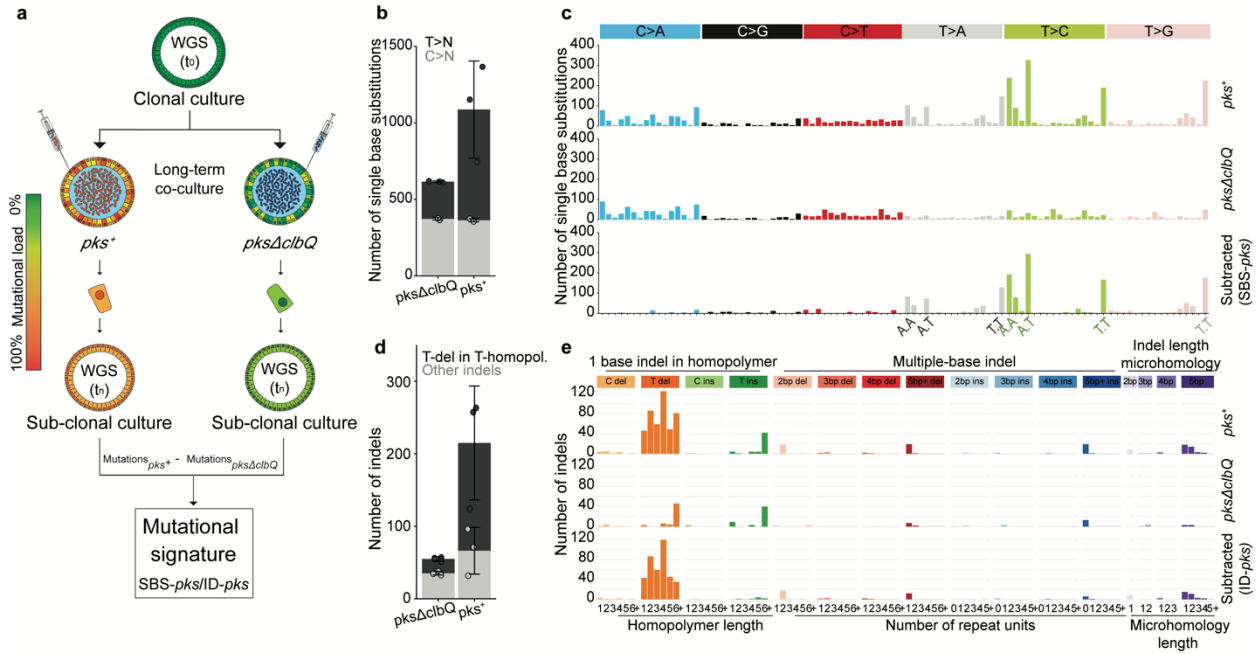
586
587
588
589
590
591
592
593
594
595
596



597 **Figure 1. Co-culture of healthy human intestinal organoids with genotoxic *E. coli* induces**
598 **DNA damage.** **a**, Schematic representation of genotoxic *E. coli* microinjection into the lumen of
599 human intestinal organoids. **b**, Scanning electron microscopy image illustrating direct contact
600 between organoid apical side and *pks*⁺ *E. coli* after 24h co-culture. Scale bar = 10 μm. **c**, Bacterial
601 load of *pks*⁺ or *pksΔclbQ* at 0, 1, 2 and 3 days after co-culture establishment (n = 8 co-cultures
602 per condition and timepoint, except *pks*⁺ d2 (n = 7) and *pksΔclbQ* d3 (n = 6)). CFU, colony forming
603 units. Center line indicates mean, error bars represent SD. **d**, Representative images of DNA
604 damage induction after 1 day of co-culture, measured by γH2AX immunofluorescence. One
605 organoid is shown per image with one nucleus in the inset. Yellow boxes indicate inset area.
606 Scale bars represent 10 μm (large image) and 2 μm (inset). **e**, Quantification of (d): Percentage
607 of nuclei positive for γH2AX foci in *pks*⁺ (n= 9 organoids), *pksΔclbQ* (n=7 organoids), dye (n=7
608 organoids) and mitomycin C (MMC) (n=7 organoids) after 1 day of co-culture. Center line indicates
609 mean, error bars represent SD.

610
611

612



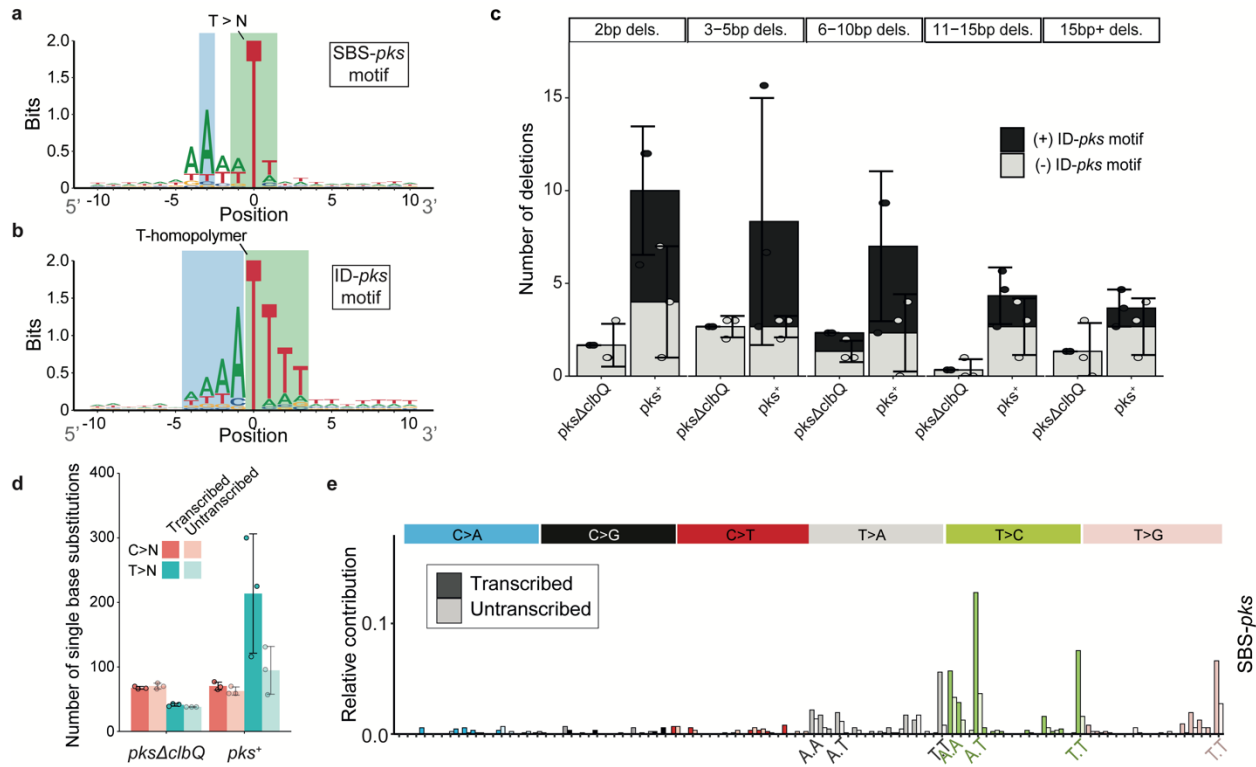
613

614

615 **Figure 2. Long-term co-culture of *pks*⁺ *E. coli* induces SBS-*pks* and ID-*pks* mutational**
 616 **signatures. a**, Schematic representation of the experimental setup. **b**, The number of single base
 617 substitutions (SBS) that accumulated in organoids co-cultured with either *pks*⁺ or *pks*Δ*clbQ* *E. coli*
 618 (*n* = 3 clones). Box height indicates mean number of events, error bars represent SD. **c**, SBS 96-
 619 trinucleotide mutational spectra in organoids exposed to either *pks*⁺ (top) or *pks*Δ*clbQ* (middle) *E.*
 620 *coli*. The bottom panel depicts the SBS-*pks* signature, which was defined by subtracting *pks*Δ*clbQ*
 621 from *pks*⁺ SBS mutations. **d**, The number of small insertions and deletions (indels) that
 622 accumulated in organoids co-cultured either with *pks*⁺ or *pks*Δ*clbQ* *E. coli* (*n* = 3 clones). Box
 623 height indicates mean number of events, error bars represent SD. **e**, Indel mutational spectra
 624 observed in organoids exposed to either *pks*⁺ (top) or *pks*Δ*clbQ* (middle) *E. coli*. The bottom panel
 625 depicts the ID-*pks* signature, which was defined by subtracting *pks*Δ*clbQ* from *pks*⁺ indel
 626 mutations.

627

628



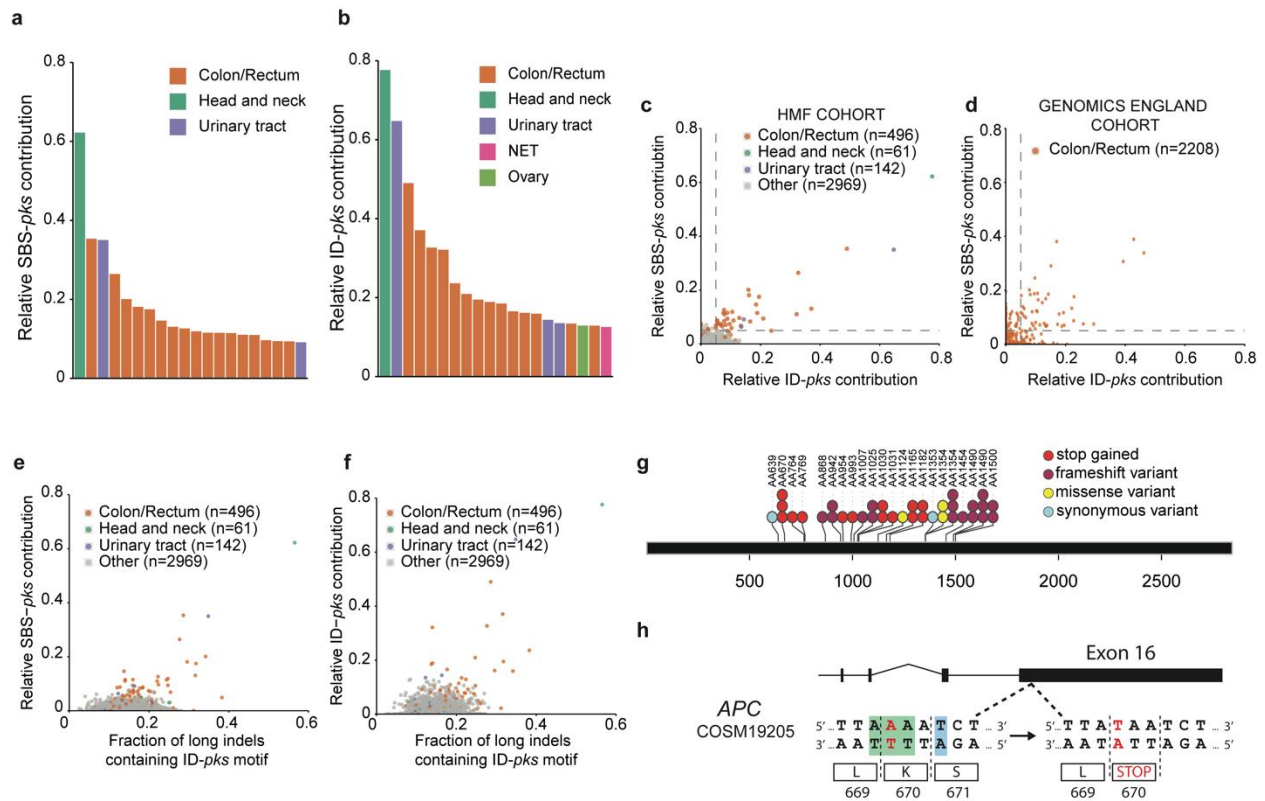
629

630

631 **Figure 3. Consensus motifs and extended features of SBS-*pks* and ID-*pks* mutational**
 632 **signatures. a**, 2-bit representation of the extended sequence context of T>N mutations observed
 633 in organoids exposed to *pks*⁺ *E. coli*. Sequence directionality indicated in grey. Green: Highlighted
 634 T>N trinucleotide sequence; Blue: Highlighted A-enriched position characteristic of the SBS-*pks*
 635 mutations. **b**, 2-bit representation of the extended sequence context of single T-deletions in T-
 636 homopolymers observed in organoids exposed to *pks*⁺ *E. coli*. Sequence directionality indicated
 637 in grey. Green: Highlighted T-homopolymer with deleted T; Blue: Highlighted characteristic poly-
 638 A stretch. **c**, Mean occurrence of < 1 base pair deletions in *pks*⁺ or *pks*Δ*clbQ* exposed organoids.
 639 Black bars correspond to deletions matching the ID-*pks* extended motifs; Grey bars correspond
 640 to deletions where no ID-*pks* motif is observed. Box height indicates mean number of events,
 641 error bars represent SD (n = 3 clones). **d**, Transcriptional strand-bias of T>N and C>N mutations
 642 occurring in organoids exposed to *pks*⁺ *E. coli* and *pks*Δ*clbQ* *E. coli*. Pink: C>N; Blue: T>N; Dark
 643 color: Transcribed strand; Bright color: Untranscribed strand. Box height indicates mean number
 644 of events, error bars represent SD (n = 3 clones). **e**, Transcriptional strand bias of the 96-
 645 trinucleotide SBS-*pks* mutational signature. Color: Transcribed strand; White: Untranscribed
 646 strand.

647

648



649

Figure 4. SBS-*pks* and ID-*pks* mutational signatures are present in a subset of CRC samples from 2 independent cohorts. **a**, Top 20 out of 3668 metastases from the HMF cohort, ranked by the fraction of single base substitutions attributed to SBS-*pks*. CRC metastases (in orange) are enriched. Colors indicate tissue of origin. **b**, Top 20 out of 3668 metastases from HMF cohort. Samples are ranked by the fraction of indels attributed to ID-*pks*. CRC metastases (in orange) are also here enriched. NET indicates neuroendocrine tumor. Colors indicate tissue of origin. **c**, Scatterplot of fraction of single base substitutions and indels attributed to SBS-*pks* and ID-*pks* in 3668 metastases. Each dot represents one metastasis. Samples high for both SBS-*pks* and ID-*pks* (> 5% contribution, dashed lines) are enriched in CRC (orange). SBS-*pks* and ID-*pks* are correlated ($R^2 = 0.46$; only CRC, $R^2 = 0.7$). Colors indicate tissue of origin. **d**, Scatterplot of SBS-*pks* and ID-*pks* contribution in 2208 CRC tumor samples, predominantly of primary origin, from the Genomics England cohort. SBS-*pks* and ID-*pks* are correlated ($R^2 = 0.35$). Each dot represents one primary tumor sample. Dashed lines delimitate samples with high SBS-*pks* or ID-*pks* contribution (> 5%). **e**, Scatterplot of SBS-*pks* and > 1 bp indels with ID-*pks* pattern in the HMF cohort. Colors indicate tissue of origin. **f**, Scatterplot of ID-*pks* and >1 bp indels with ID-*pks* pattern in the HMF cohort. Colors indicate tissue of origin. **g**, Exonic APC driver mutations found in the IntOGen collection matching the colibactin target SBS-*pks* or ID-*pks* motifs. **h**, Schematic representation of a driver mutation in APC causing a premature stop codon matching the SBS-*pks* motif, found in the IntOGen collection and in two independent SBS/ID-*pks* high patients from the HMF cohort.

670

671

672 **Extended Data Fig. 1. Co-culture with genotoxic *pks*⁺ *E. coli* induces DNA interstrand**
673 **crosslinks in healthy human intestinal organoids. a**, Representative images (out of n = 5
674 organoids per group) of DNA interstrand crosslink formation after 1d of co-culture, measured by
675 FANCD2 immunofluorescence (green). Nuclei were stained with DAPI (blue). Yellow boxes
676 represent inset area. Scale bars represent 50 μ m (large image) and 10 μ m (inset). Experiment
677 was repeated independently twice with similar results. **b**, Gating strategy to select epithelial cells
678 (left) and to quantify viable cells (right). **c**, Viability of intestinal organoid cells after 1, 3 and 5 days
679 of co-culture (n = 3 technical replicates) (bacteria eliminated after 3 days of co-culture). Points
680 are independent replicates, center line indicates mean, error bars represent SD.

681

682

683 **Extended Data Fig. 2. Genotoxic *pks*⁺ *E. coli* induce SBS-*pks* and ID-*pks* mutational**
684 **signatures after long-term co-culture with wild-type intestinal organoids. a,** 96-trinucleotide
685 mutational spectra of SBS in each of the 3 individual clones sequenced per condition. Top 3: dye;
686 middle 3: *pks* Δ *clbQ* *E. coli*; bottom 3: *pks*⁺ *E. coli*. **b,** Total 96-trinucleotide mutational spectra of
687 *pks*⁺ and *pks* Δ *clbQ* from which dye single base substitutions are subtracted. **c,** Heatmap depicting
688 cosine similarity between dye, *pks*⁺ *E. coli* and *pks* Δ *clbQ* *E. coli* 96-trinucleotide mutational
689 profiles. **d,** Indel mutational spectra plots from each of the 3 individual clones sequenced per
690 condition. Top 3: dye; middle 3: *pks* Δ *clbQ* *E. coli* bottom 3: *pks*⁺ *E. coli* **e,** Total indel mutational
691 spectra of values of *pks*⁺ *E. coli* and *pks* Δ *clbQ* *E. coli* from which dye indels are subtracted. **f,**
692 Heatmap depicting cosine similarity between dye, *pks*⁺ *E. coli* and *pks* Δ *clbQ* *E. coli* indel
693 mutational profiles.

694

695

696 **Extended Data Fig. 3. Genotoxic *pks*⁺ *E. coli* and isogenic strain reconstituted with**
697 ***pks*Δ*clbQ*:*clbQ* induce SBS-*pks* and ID-*pks* mutational signatures after co-culture. a,** 96-
698 trinucleotide mutational spectra of SBS in 3 individual clones from the independent human healthy
699 intestinal organoid line ASC 6-a co-cultured for 3 rounds with *pks*⁺ or *pks*Δ*clbQ* *E. coli*. **b,** Top:
700 Total 96-trinucleotide mutational spectrum from the 3 clones from *pks*⁺ or *pks*Δ*clbQ* *E. coli* shown
701 in (a). Bottom: Resulting 96-trinucleotide mutational spectrum from ASC 6-a co-cultured with *pks*⁺
702 *E. coli* after the subtraction of background mutations from 3 parallel *pks*Δ*clbQ* *E. coli* co-cultures
703 (cosine similarity to SBS-*pks* = 0.77). **c,** Indel mutational spectra plots from the 3 independent
704 ASC 6-a clones co-cultured for 3 rounds with *pks*⁺ or *pks*Δ*clbQ* *E. coli*. **d,** Top: Total indel
705 mutational spectrum from the 3 clones from *pks*⁺ or *pks*Δ*clbQ* *E. coli* shown in (c). Bottom:
706 Resulting indel mutational spectrum from the independent ASC 6-a co-cultured with *pks*⁺ *E. coli*
707 after the subtraction of background mutations from 3 parallel *pks*Δ*clbQ* *E. coli* co-cultures (cosine
708 similarity to ID-*pks* = 0.93). **e,** 96-trinucleotide mutational spectrum from 3 individual clones of the
709 ASC 5-a line co-cultured for 3 rounds with the isogenic recomplemented strain *pks*Δ*clbQ*:*clbQ*. **f,**
710 Top: Total 96-trinucleotide mutational spectrum from the 3 clones from *pks*Δ*clbQ*:*clbQ* shown in
711 (e). Bottom: Resulting mutational spectrum after subtracting *pks*Δ*clbQ* background (cosine
712 similarity to SBS-*pks* = 0.95). **g,** Indel mutational spectrum from 3 individual clones of the ASC 5-
713 a line co-cultured for 3 rounds with the isogenic recomplemented strain *pks*Δ*clbQ*:*clbQ*. **h,** Top:
714 Total indel mutational spectrum from the 3 clones from *pks*Δ*clbQ*:*clbQ* shown in (e). Bottom:
715 Resulting mutational spectrum after subtracting *pks*Δ*clbQ* background (cosine similarity to ID-*pks*
716 = 0.95).

717

718

719 **Extended Data Fig. 4. Detailed sequence context for ID-*pks* and longer deletions by length.**
720 **a**, 10 base up- and downstream profile shows an upstream homopolymer of adenosines favoring
721 induction of T-deletions. The length of the adenosine stretch decreases with increasing T-
722 homopolymer length (1—8, top left to bottom right).

723

724

725 **Extended Data Fig. 5. Signature extraction and clonal contribution of SBS-*pks* in CRC**
726 **metastases. a**, *De-novo* extracted NMF-SBS-*pks* signature by non-negative matrix factorization
727 (NMF) on all 496 CRC metastases in the HMF dataset. **b**, Cosine similarity scores between the
728 *de-novo* extracted SBS signature in (a) and COSMIC SigProfiler signatures, including our
729 experimentally defined SBS-*pks* signature (left). **c**, Relative contribution of SBS-*pks* to clonal
730 (corrected variant allele frequency > 0.4, blue bar) and subclonal fraction (corrected variant allele
731 frequency < 0.2, red bar) of mutations in the 31 SBS/*ID-pks* high CRC metastases from the HMF
732 cohort. Box indicates upper and lower quartiles with the center line indicating the mean. Box
733 whiskers: largest value no further than 1.5 times the interquartile range extending from the box.
734 Points indicate individual CRC metastases.